Supporting Information

Crisman et al. 10.1073/pnas.0908570106

SI Materials and Methods

Structural Alignments. Structural alignments were carried out between different fragments of the GltPh structure using the program SKA (1). To identify significant structural relationships, we only considered segments with a minimum of three secondary structure elements. It was assumed that the two helical hairpins, given their clear structural relationship, would constitute the basis of one repeat. Extending the segment containing HP2 as much as possible toward the C terminus, which optimizes the coverage of the structure, creates a unit consisting of HP2 and TM8. The two half-helices of TM7, when considered as one single helix, together with HP1, provide an analogous region that has the opposite topology. A relationship between TM7 an TM8 is supported by their structural alignment using TMalign (2), which has a rmsd of 1.7 Å (Table S1). The structural superposition of HP1+TM7 and HP2+TM8 (Fig. 2*A*) with SKA has a protein structure distance score of ≈1.0, which is within the range observed for proteins classified as in the same "family" according to the Structural Classification of Proteins database (3).

N-terminal to the hairpins are six membrane-spanning helices and two nontransmembrane helices. The possible combinations of segments of at least three secondary structure elements with inverted topologies are limited to TMs 1 to 3 and TMs 4 to 6. However, because TM4 contains three separate helices, we tested the effect of including the different helical segments of TM4. The most reasonable structural alignment was obtained when TM4c was considered to be equivalent to TM1 (see Table S1 and Fig. 2*B*). Helices 4a and 4b are therefore considered to be part of a long loop between the repeats, which is consistent with the long sequence insertion found in this region in human EAAT homologs. The main difference between TMs 1 to 3 and TMs 4c to 6 is that TMs 2 and 5 are curved in opposite directions.

Alignment of Repeat Sequences. To construct a model in which the conformations of the repeats were swapped, it was necessary to generate pairwise sequence alignments between segments I and II, and between segments III and IV. For the former, alignments were extracted from the structural alignment of those segments using SKA (1). That is, residues that were closest to one another in space after the structural superposition were assumed to be aligned. For segments III and IV, we found that pairwise sequence alignments resulted in fewer gaps in the helices, and we thus used ClustalW (4) to align HP1 with HP2 (≈16% identity) and TM7 with TM8 (≈20% identity). The complete alignment was constructed according to Fig. 3 (Fig. S1*A*). A few gaps were manually removed from the alignments of TMs 2, 3, 5, and 6, so that these helices would be modeled as continuous helices, and a preliminary model of a protomer was constructed from this alignment (Fig. S1*C*).

Optimization of Alignment. As can be seen from Fig. S1*C*, the preliminary model demonstrates the same major conformational change described for the final model (Fig. S1*D*). Refinements were made to this model, to: (*i*) match the secondary structure observed the crystal structure with helical regions in the template as far as possible; (*ii*) reproduce the rotational (pitch) or translational (height) position of individual helices with respect to the membrane, aqueous solution or to other helices in the protein; and (*iii*) maintain the relative positions of binding site residues. These refinements create a more realistic model from physical-chemical and biological perspectives, and allow for a simpler comparison with the x-ray structure, while not affecting the major conformational change. They can be considered reasonable given the difficulty of accurate sequence and structural alignments at low sequence identities.

Specifically, the adjustments to the alignment were:

- The alignment of TMs 1, 2, and 3 was shifted by four residues (one helix turn) to increase the template coverage.
- The alignment of TM4c and TM5 was adjusted by four residues to maintain the contacts between protomers in the trimer, which are believed not to change during transport (5). These contacts are between TM2 and helix 4a (residue pairs L49:L135 and K55:T140), between helices 4b of neighboring protomers (F143:A147 and G144:A147), between helix 4c and TM5 (A164:A193 and A164:K196), and between TMs 5 of neighboring protomers (S179:D185, S179:N188, T182:D185 and L183:A186).
- The alignment of the C-terminal half of TM6 was adjusted by one residue to remove an insertion in the TM domain.
- The alignment of HP1 was shifted by one to two residues, to remove a gap in HP1a and to place residues 276 to 279 at the tip of the hairpin (see Fig. S1 *C* and *D*).
- The binding-site residues 308 to 313 in TM7 were modeled without template and instead constraints were applied (see below).
- The alignment of HP2a was shifted by one residue to remove an insertion in the helix, while keeping residues 352 to 357 at its tip. An insertion was accommodated at the tip of this hairpin because the template contains fewer uncoiled residues.
- The alignment of the C-terminal half of TM8 was shifted by three residues to optimize the template coverage, while maintaining its helical pitch as in the crystal structure (e.g., with respect to TM7). Similarly, the alignment of the N-terminal half of TM8 was shifted by four residues. No template was used for residues 373 to 379 in the center of TM8, because the corresponding region is uncoiled, and instead constraints were applied (see below).

Importantly, none of these adjustments altered the overall shape of the model, and the essential features—namely the large shift of a domain containing HP1/TM7/HP2/TM8, as well as exposure of HP1 and burial of HP2—were conserved (see Fig. S1 *C* and *D*). This is because, in both models, the same TM helices are aligned to one another, while only the relative position of individual residues along those helices is changed.

The final alignment (Fig. S2) has a sequence identity of 9.8% (excluding 3L4).

Construction of Protomer Models. Models of GltPh protomers were built using the optimized sequence alignment (see Fig. S2), using the corresponding segment as a template. The loop between TMs 3 and 4 (3L4), including helices 4a and 4b (residues 111–149), which is not repeated, was kept the same as in PDB structure 2NWL. This was achieved by repositioning these residues in the template to the desired location of the loop in the final model. To further conserve the internal structure of the protomer (binding-site residues, orientation of individual helices, location of interface residues, and secondary structure), we added constraints for segments in which the template differed slightly from the x-ray structure. These constraints were taken from the x-ray structure using a cut-off distance of 6 Å. Specifically, we constrained:

- All residues in 3L4/TM4/TM5 (all atoms in residues 123–229), to fix the position of helices 4a and 4b within the interface (according to the constraints implied by ref. 5), and to improve the helicity of the cytoplasmic ends of TM4c and TM5;
- The binding-site residues in TM7 (between Cα atoms of residues 309–312);
- The internal structure of HP1 (between Cα atoms of the following residue pairs: 271 and 281, 268 and 284, 265 and 288, 275 and 281, as well as between Cα and Cβ atoms of residues 267–301);
- The relative orientation of the top of TM5 with respect to TM8 (between Cα atoms in residue 383 and in residues 208, 212, 216, and 220); and
- The helicity of the following regions: HP1a (residues 258–275), HP1b (residues 278–292), TM7 (residues 296–309 and 312–329), and TM8 (residues 386–401).

As can be seen from Fig. S1*D*, these changes serve to retain the internal structure of untemplated segments of the protomer, while not altering the relative movements of the repeats or the overall conformational change.

When using aspartate-bound GltPh as the template (PDB code 2NWL), 5,000 models were constructed, and the model with the lowest Modeller score was selected for further analysis. According to Procheck (6), four (1.2%) and three (0.9%) residues are in the generously allowed and disallowed regions, respectively, of the Ramachandran plot for this model. For a second model, built using the TBOA-bound structure of GltPh (PDB code 2NWW) as a template, the selected model from 2,000 attempts has equivalent Procheck values of five (1.4%) and four (1.2%), respectively.

Construction of Trimer Model. To construct trimeric models, we fitted the protomers onto the x-ray structure using helices TM3, 4a, 4b, TM4c, TM5, and TM6 (Cα atoms of residues 82–253). This maintained interfacial contacts in accordance with cross-linking experiments in GltT (5), and minimized changes at the protein-lipid interface. All atoms in the interfacial residues 137 to 147, as well as all side chains, were energy minimized with steepest descents for 2,000 steps using Charmm (7). The trimer models are deposited with identifiers PM0075966 (2NWL-based model) and PM0075968 (2NWW-based model) in the Protein Model Database (8) at http://mi.caspur.it/PMDB.

Transport Measurements. Uptake of D-[^{3}H]aspartate was performed essentially as described (9), after pretreatment with DTT or CuPh as follows: for each condition, five oocytes were washed twice with 1 ml of frog Ringer's solution containing 96-mM NaCl, 2-mM KCl, 1.8-mM $CaCl_2$, 1-mM $MgCl_2$, 5-mM Hepes, pH 7.5 and were subsequently incubated for 5 min with 1 ml of the same solution supplemented with 5 mM of DTT. Subsequently, the oocytes were washed twice with solutions of the compositions indicated in the figure legends, followed by a 5-min incubation of the oocytes with the same solution supplemented with 100 μM of CuPh. After washing the oocytes twice in frog Ringer's solution, the oocytes were incubated for 20 min in 500 μl of the same solution supplemented with 1 μCi of D-[^{3}H]aspartate (uptake was linear for at least 30 min). The oocytes were washed by passing through four wells filled with 4 ml frog Ringer's solution followed by the individual incubation of each oocyte in 1% of SDS (500 μl/oocyte), followed by liquid scintillation counting. Each experiment was performed with two or three different batches of oocytes.

1. Petrey D, et al. (2003) Using multiple structure alignments, fast model building, and energetic analysis in fold recognition and homology modeling. *Proteins* 53:430–435.
2. Zhang Y, Skolnick J (2005) TM-align: a protein structure alignment algorithm based on the TM-score. *Nucl Acids Res* 33:2302–2309.
3. Yang AS, Honig B (2000) An integrated approach to the analysis and modeling of protein sequences and structures. I. Protein structural alignment and a quantitative measure for protein structural distance. *J Mol Biol* 301:665–678.
4. Thompson JD, Higgins DG, Gibson TJ (1994) CLUSTAL_W: improving the sensitivity of progressive multiple sequence alignment through sequence weighting, position-specific gap penalties and weight matrix choice. *Nucl Acids Res* 22:4673–4680.
5. Groeneveld M, Slotboom D-J (2007) Rigidity of the subunit interfaces of the trimeric glutamate transporter GltT during translocation. *J Mol Biol* 372:565–570.
6. Laskowski RA, Macarthur MW, Moss DS, Thornton JM (1993) PROCHECK - A program to check the stereochemical quality of protein structures. *J Appl Crystall* 26:283–291.
7. Brooks BR, et al. (1983) CHARMM: A program for macromolecular energy, minimization, and dynamics calculations. *J Comput Chem* 4:187–217.
8. Castrignanò T, et al. (2006) The PMDB Protein Model Database. *Nucl Acids Res* 34:D306–D309.
9. Bendahan A, Armon A, Madani N, Kavanaugh MP, Kanner BI (2000) Arginine 447 plays a pivotal role in substrate interactions in a neuronal glutamate transporter. *J Biol Chem* 275:37436–37442.

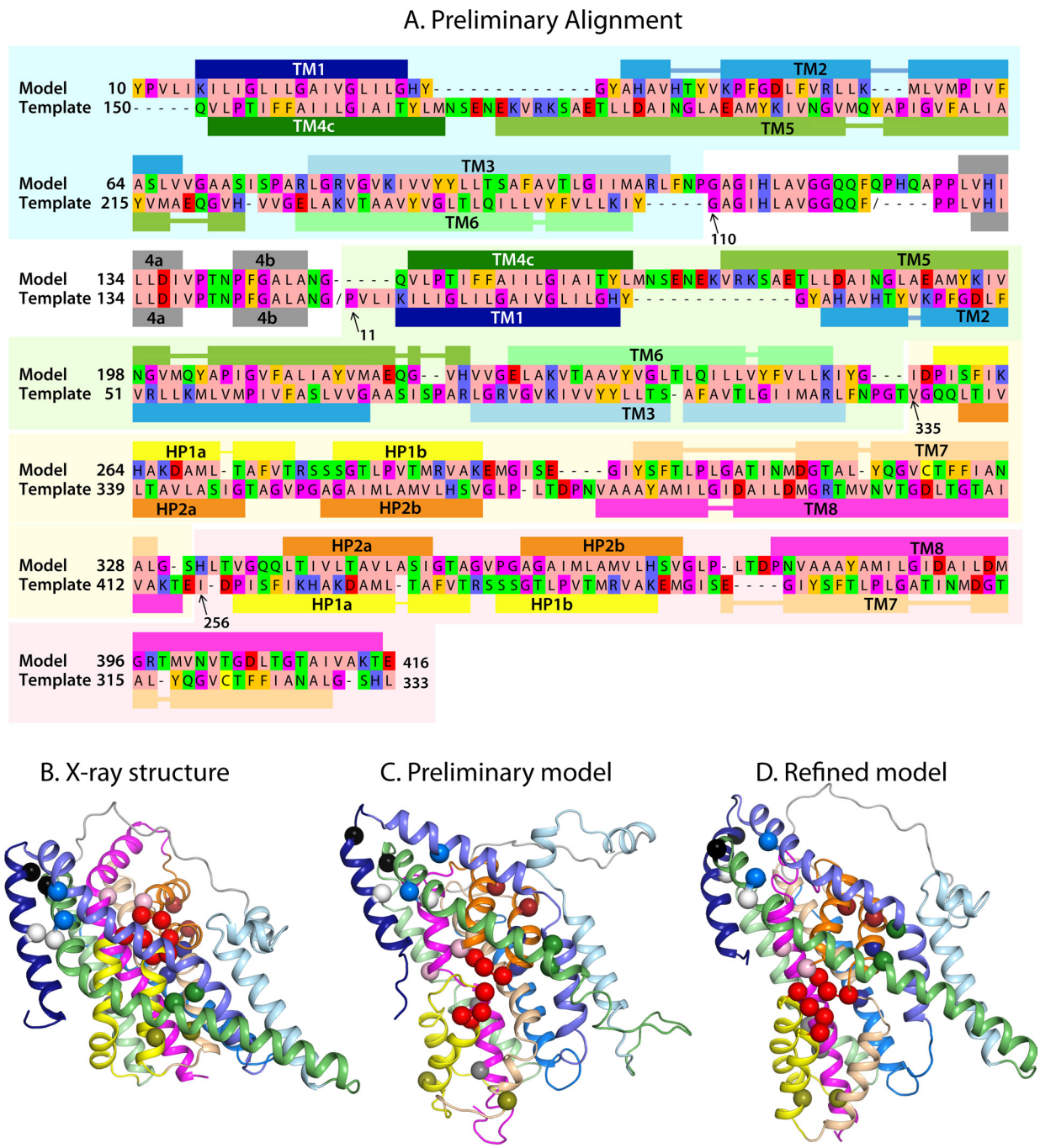

Fig. S1. Construction of the model of GltPh. (*A*) Preliminary sequence alignment between model and template sequences for internal-repeat homology modeling of GltPh. The alignment was constructed from the SKA structural alignment of segments I and II, and the ClustalW alignments of HP1 with HP2 and of TM7 with TM8, from which gaps in TMs 2, 3, 5, and 6 were removed (see *SI Materials and Methods*). Known TM helical segments according to PDB structure 2NWL are shown above and below the alignment for the model and template sequences, respectively. The helices are colored as in Fig. 3. A preliminary model of GltPh (*C*) was constructed using this alignment, and was compared to the x-ray structure (*B*) to guide adjustments of the alignment, which resulted in a refined model (*D*). For example, residues that are helical in the x-ray crystal structure were aligned wherever possible with residues that are helical in the corresponding part of the repeat [e.g., the cytoplasmic end of TM8 (magenta) is more helical in the final model than in the preliminary model]. The Cα atoms of pairs of specific residues from adjacent TM regions (shown as spheres of the same color) were used to help adjust the pitch/orientation of individual helices. For example, the alignment of residues in the tip of HP1 (red spheres) was incorrect in the preliminary model and was refined for the final model.

Fig. S2. Refined alignment between model and template sequences for internal-repeat homology model of GltPh. Coloring as shown in Fig. S1.

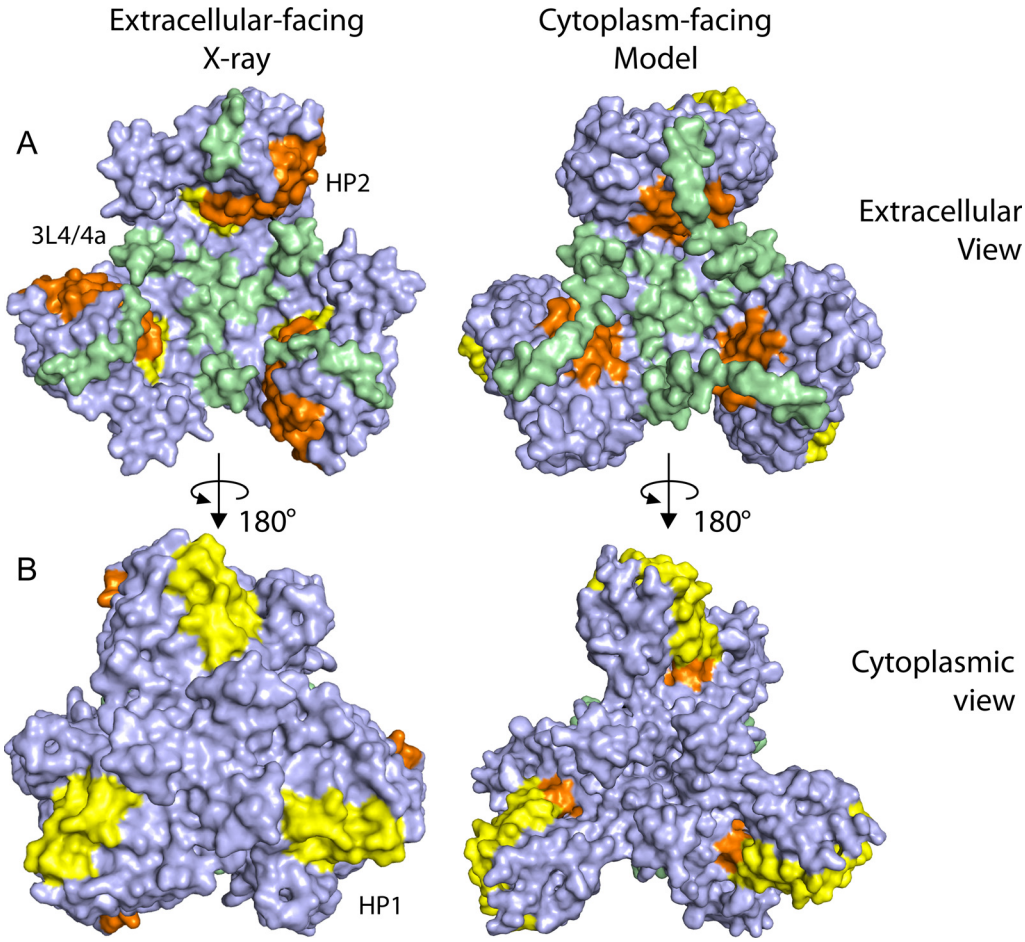

Fig. S3. The surface of the GltPh trimer in the extracellular-facing x-ray structure (*Left*) and the model of the cytoplasm-facing conformation (*Right*), viewed from extracellular (*A*) and cytoplasmic (*B*) sides of the membrane, with HP1 in yellow and HP2 in orange. The 3L4 loop and helix 4a are colored light green for reference. The tip of HP1 is exposed to the extracellular solution in the x-ray structure, but not in the model; analogously, the tip of HP2 is exposed to the cytoplasm only in the inward-facing model.

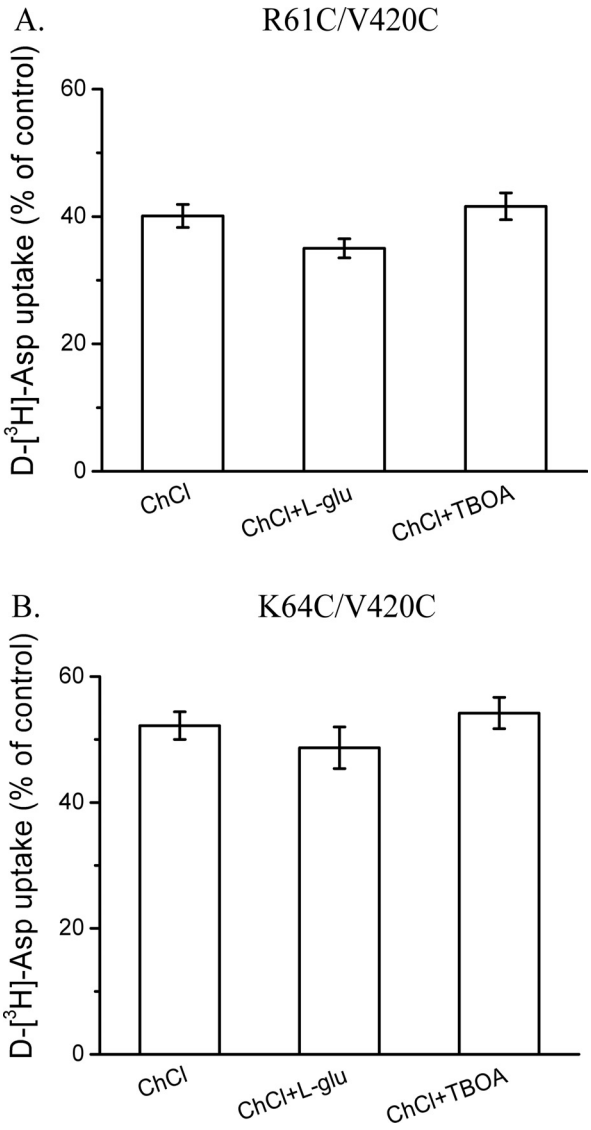

Fig. S4. Effect of CuPh treatment in the absence of sodium on the transport activity of R61C/V420C and K64C/V420C. After pretreatment of the oocytes expressing R61C/V420C (*A*) or K64C/V420C (*B*) with 5-mM DTT for 5 min, as described in *SI Materials and Methods*, the oocytes were washed with frog Ringer's solution in which all of the NaCl was replaced by ChCl. This was followed by incubation with 100-μM CuPh with the same solution in the absence or presence of either 1-mM L-glutamate or 60 μM of TBOA. Subsequently, sodium-dependent radioactive D-aspartate transport was measured, as described in *SI Materials and Methods*. The results are expressed as a percentage of activity of oocytes incubated without CuPh.

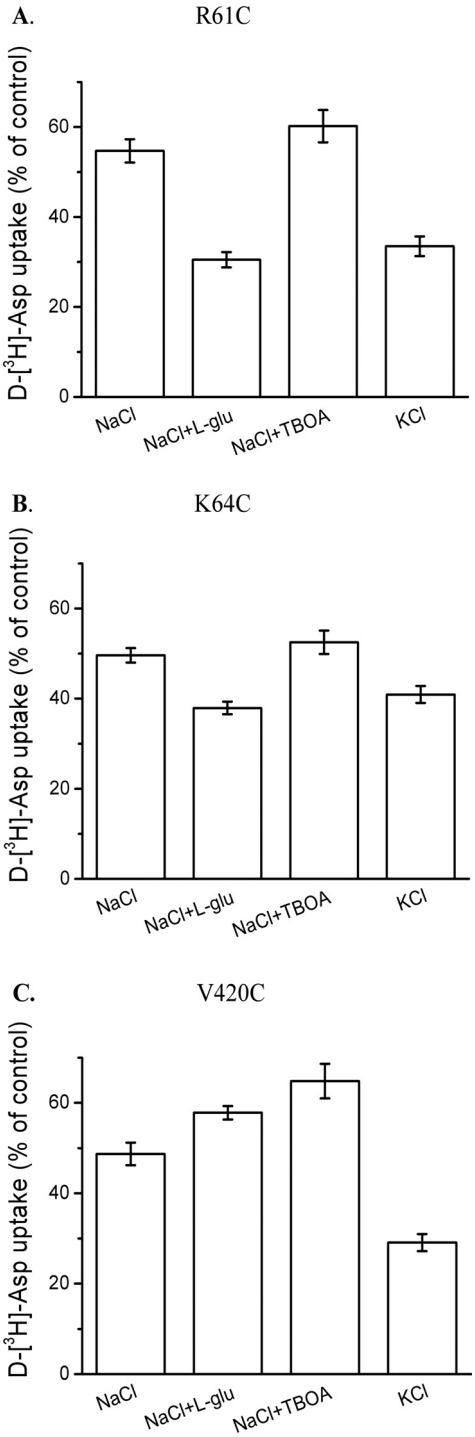

Fig. S5. Effect of the medium composition during treatment with MTS reagents on the transport activity of R61C, K64C and V420C. Oocytes expressing R61C (*A*), K64C (*B*), or V420C (*C*) were first washed with frog Ringer's solution in the absence or presence of either 1-mM L-glutamate or 60-μM TBOA, or in frog Ringer's solution in which all of the NaCl was replaced by KCl. The oocytes were then incubated for 5 min in solutions of the same compositions in the presence or absence of 10-mM MTSES (*A* and *B*) or 0.02-mM MTSET (*C*), followed by washing in frog Ringer's solution, and then by transport measurements as described in *SI Materials and Methods*. The concentrations of MTSES and MTSET were chosen after preliminary titration experiments, to determine the concentration required for ≈50% inhibition in sodium-containing medium for each mutant. This level of inhibition is optimal for determining the effect of the medium composition on the sensitivity of the cysteine mutants to sulfhydryl reagents. The results are expressed as the percentage of transport activity of oocytes incubated without MTS reagents.

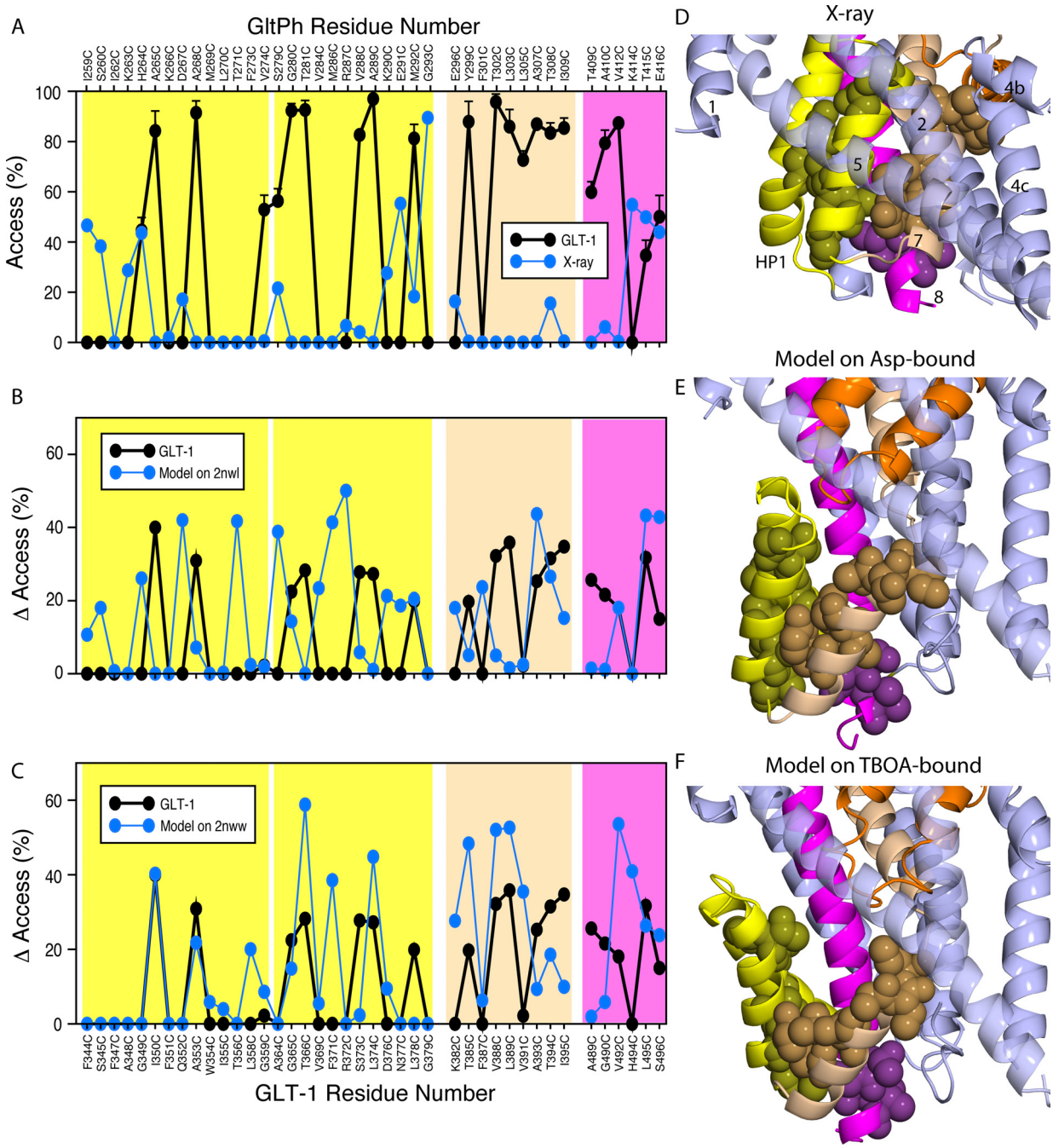

Fig. S6. Increase in accessibility in HP1 (yellow), TM7 (wheat), and TM8 (pink) in the inward-facing model of GltPh is supported by cysteine accessibility measurements in GLT-1. (*A*) The reduction of glutamate uptake by NEM in single-cysteine mutants in the presence of potassium, as a percentage of uptake in the absence of NEM (in black) is a measure of the absolute accessibility in the inward-facing conformation (1). The calculated solvent accessible surface area of the equivalent residues of GltPh in an outward-facing conformation (PDB code 2NWL) is in blue. This accessibility was calculated as a percentage of the accessibility of the same amino acid type (X) in a reference GXG tripeptide (as described in ref. 2). (*B* and *C*) The increase in accessibility for inward-facing models of GltPh relative to the crystal structure (blue) is compared to the effect of extracellular potassium relative to sodium on the inhibition by NEM (black). The latter was calculated by subtracting the percentage inhibition by potassium from the inhibition by sodium. Models were built using either (*B*) an aspartate-bound structure (PDB code 2NWL), or (*C*) a TBOA-bound structure (PDB code 2NWW), as templates. In all plots, negative values have been set to zero. (*D–F*) Positions equivalent to residues that become significantly more accessible upon addition of potassium in GLT-1 (spheres) are shown in the x-ray structure (*D*), and in inward-facing models of GltPh built using a glutamate-bound structure (*E*) or a TBOA-bound structure (*F*).

1. Shlaifer I, Kanner BI (2007) Conformationally sensitive reactivity to permeant sulfhydryl reagents of cysteine residues engineered into helical hairpin 1 of the glutamate transporter GLT-1. *Mol Pharmacol* 71:1341–1348. 2. Forrest LR, et al. (2008) A mechanism for alternating access in neurotransmitter transporters. *Proc Natl Acad Sci USA* 105:10338–10343.

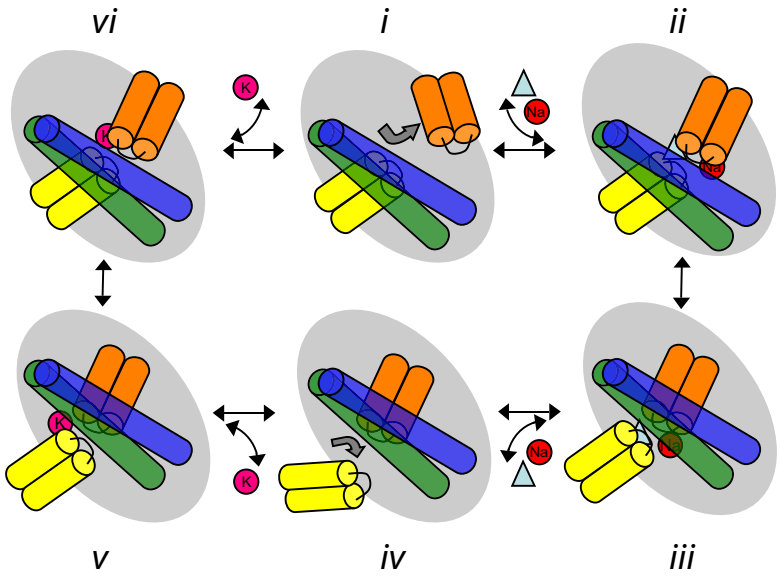

Fig. S7. Proposed mechanism of glutamate/aspartate transport involving four major conformational states of the protein. TM 2 (*blue*), TM 5 (*green*), HP1 (*yellow*), and HP2 (*orange*) from one subunit are shown for clarity. Substrate is shown as a light blue triangle and ions are shown as colored spheres. The four states are: (*i*) outward-facing open; (*ii* and *vi*) outward-facing occluded; (*iii* and *v*) inward-facing occluded; and (*iv*) inward-facing open. Nontransportable analogues bind to GltPh to form a conformation similar to (*i*), and the aspartate/sodium-bound structures of GltPh correspond to (*ii*). Here, we propose atomistic models for states (*iii*) and (*iv*) and for the conformational change connecting (*ii*) and (*iii*).

Table S1. Structural similarities of fragments of GltPh

Fragment 1		Fragment 2		Similarities	
Name	Residues	Name	Residues	RMSD, Å	PSD
HP1	256–293	HP2	336–373	2.6*	0.44
TM7	294–335	TM8	374–420	1.7*	0.49
HP1 + TM7	256–335	HP2 + TM8	336–420	4.8	0.99
TM1–3	10–110	TM4a-6	125–255	4.6	0.88
TM1–3	**10–110**	**TM4c-6**	**150–255**	**4.3**	**0.76**
TM1–3 + HP2 + TM8	10–110 and 336–420	TM4c-6 + HP1 + TM7	150–335	4.6	0.89

Boldface indicates a structural alignment from which the sequence alignment was extracted to be used in the homology modeling. TM-scores of >0.4 indicate that the segments provide homology modeling templates defined as ''Easy'' [Zhang Y, Skolnick J (2004) Scoring function for automated assessment of protein structure template quality. *Proteins* 57:702–710.].

*Structure alignments calculated with TM-align instead of SKA, because they contained <3 secondary structure elements. Here, PSD is replaced by the TM-score.